

AD-A269 572



NASA Technical Memorandum 106189  
AIAA-93-1797

Army Research Laboratory  
Memorandum-ARL-MR-91

# Measurements and Computational Analysis of Heat Transfer and Flow in a Simulated Turbine Blade Internal Cooling Passage

Louis M. Russell  
*National Aeronautics and Space Administration  
Lewis Research Center  
Cleveland, Ohio*

Douglas R. Thurman  
*Vehicle Propulsion Directorate  
U.S. Army Research Laboratory  
Lewis Research Center  
Cleveland, Ohio*

Patricia S. Simonyi  
*Sverdrup Technology, Inc.  
Lewis Research Center Group  
Brook Park, Ohio*

and

Steven A. Hippensteele and Philip E. Poinsette  
*National Aeronautics and Space Administration  
Lewis Research Center  
Cleveland, Ohio*

DTIC  
ELECTE  
SEP 15 1993  
E D

THE STATE  
Approved for public release  
Distribution Unlimited

93-21309



Prepared for the  
29th Joint Propulsion Conference and Exhibit  
cosponsored by the AIAA, SAE, ASME, and ASEE  
Monterey, California, June 28-30, 1993



"Original contains color  
plates: All DTIC reproductions  
will be in black and  
white"



92  
CCL U ULA OMS/2



**AIAA-93-1797**

**Measurements and Computational Analysis of Heat Transfer and Flow in a Simulated Turbine Blade Internal Cooling Passage**

Louis M. Russell, Steven A. Hippensteele, and Philip E. Poinatte

NASA Lewis Research Center  
Cleveland, OH

Douglas R. Thurman  
Vehicle Propulsion Directorate  
U.S. Army Research Laboratory  
NASA Lewis Research Center  
Cleveland, OH

and  
Patricia S. Simonyi  
Sverdrup Technology, Inc.  
NASA Lewis Research Center Group  
Cleveland, OH

Accession For	
NTIS	<input checked="" type="checkbox"/>
CRA&I	<input type="checkbox"/>
DTIC	<input type="checkbox"/>
TAB	<input type="checkbox"/>
Unannounced	<input type="checkbox"/>
Justification	
By _____	
Distribution / _____	
Availability Codes	
Dist	Avail and/or Special
A-1	

DTIC QUALITY INSPECTED 1

\*Original contains color plates: All DTIC reproductions will be in black and white\*

**AIAA/SAE/ASME/ASEE**

**29th Joint Propulsion Conference and Exhibit**

June 28-30, 1993 / Monterey, CA

MEASUREMENTS AND COMPUTATIONAL ANALYSIS OF HEAT TRANSFER AND FLOW  
IN A SIMULATED TURBINE BLADE INTERNAL COOLING PASSAGE

Louis M. Russell\*  
National Aeronautics and Space Administration  
Lewis Research Center  
Cleveland, Ohio 44135

Douglas R. Thurman\*  
Vehicle Propulsion Directorate  
U.S. Army Research Laboratory  
Lewis Research Center  
Cleveland, Ohio 44135

Patricia S. Simonyi\*\*  
Sverdrup Technology, Inc.  
Lewis Research Center Group  
Brook Park, Ohio 44142

and

Steven A. Hippensteele\* and Philip E. Poinatte†  
National Aeronautics and Space Administration  
Lewis Research Center  
Cleveland, Ohio 44135

Abstract

Visual and quantitative information were obtained on heat transfer and flow in a branched-duct test section that had several significant features of an internal cooling passage of a turbine blade. The objective of this study was to generate a set of experimental data that could be used to validate computer codes for internal cooling systems.

Surface heat transfer coefficients and entrance flow conditions were measured at entrance Reynolds numbers of 45,000, 335,000, and 726,000. The heat transfer data were obtained using an Inconel heater sheet attached to the surface and coated with liquid crystals. Visual and quantitative flow field results using particle image velocimetry were also obtained for a plane at midchannel height for a Reynolds number of 45,000. The flow was seeded with polystyrene particles and illuminated by a laser light sheet.

Computational results were determined for the same configuration and at matching Reynolds numbers; these surface heat transfer coefficients and flow velocities were computed with a commercially available code. The

experimental and computational results were compared. Although some general trends did agree, there were inconsistencies in the temperature patterns as well as in the numerical results. These inconsistencies strongly suggest the need for further computational studies on complicated geometries such as the one studied.

Nomenclature

A heated area,  $m^2$   
h heat transfer coefficient,  $W/m^2 K$   
Q heat rate, W  
r recovery factor  
T temperature,  $^{\circ}C$   
 $U_{\infty}$  free-stream velocity, m/sec  
 $\nu$  kinematic viscosity,  $m^2/sec$   
 $\rho$  density,  $g/cm^3$   
 $\tau_w$  wall shear stress,  $N/m^2$

Subscripts:

e electrical heat input  
L loss  
LC liquid crystal

\*Aerospace engineer.

\*\*Research engineer.

†AIAA member, aerospace engineer.

R recovery  
s static  
t total

### Introduction

A continuing objective in gas turbine technology is higher engine efficiency. One method of obtaining higher efficiency is to use higher engine operating temperatures. Such higher turbine inlet temperatures often require the use of internal cooling in the blades and vanes to maintain surface temperatures that the material can withstand for sustained periods of time. When internal cooling is used, it is important that it be used in the most effective manner. Effective design of internal cooling passages requires an understanding of the flow and temperature patterns that occur, and it is greatly enhanced by the availability of dependable, validated computer codes.

An experimental study was performed to obtain quantitative visual information on flow and heat transfer in a test section that had several significant features of the internal passage of an experimental cooled radial turbine blade described in Ref. 1. The objective of this study was to generate a set of experimental heat transfer and flow field data that could be used to validate computer codes for internal cooling systems. In recent years, there have been several attempts to numerically model internal flow and heat transfer with computer codes.<sup>2,3</sup> Reference 2 points out that it is the combination of a complete experimental database and accurate, efficient analytical tools that will ultimately shorten design times and optimize future turbines. Reference 4 further emphasizes the importance of coordination and cooperation between experimental and computational researchers in aeropropulsion systems. Reference 5 reports on a code prediction for a rotating square duct that was verified by experimental data. Through such coordination, the results of the present study will be used to validate internal cooling codes for more complicated geometries.

Entrance velocity profiles and free-stream turbulence intensity were measured to establish upstream boundary conditions for the computations. Surface heat transfer coefficients were measured at entrance Reynolds numbers of 45,000, 335,000, and 726,000 (based on the entrance hydraulic diameter). The heat transfer data were obtained by using a uniform Inconel heater sheet attached to the test section floor and coated with thermochromic liquid crystals. Liquid crystals, by virtue of their property of changing color with temperature, provide a means of measuring surface temperature and visualizing thermal patterns at any desired location. The local heat transfer coefficients were calculated by measuring the electrical input to the heater sheet under flow

conditions and using a heat balance. Reference 6 describes the method in more detail.

Quantitative visual flow field measurements from particle image velocimetry are also presented for a plane at midchannel height and a test section entrance Reynolds number of 45,000. The flow field was seeded with 1- $\mu$ m polystyrene particles and illuminated by a laser light sheet. This flow field work is an extension of work done in conjunction with the University of Akron where the procedure and the computerized data reduction method were developed. Details of this method are given in Ref. 7. The present report includes a much larger extension of the flow field covered in Ref. 7 such that it can be compared with the heat transfer results.

Computational results for the same configuration were obtained with a commercially available code. This code was used to calculate surface heat transfer coefficients and flow field velocities at Reynolds numbers matching some of the experimental results. The experimental and computational results were compared. Although some general trends did agree, there were inconsistencies in the heat transfer patterns and magnitudes. These inconsistencies demonstrate the need for further development of computational studies on complicated geometries such as the one investigated.

### Apparatus

Figure 1 is a schematic of the complete test facility. Room temperature air was drawn through a tunnel by a vacuum exhaust system. The two-piece test section (Fig. 2) was made of clear acrylic plastic and had a passage height of 5.08 cm. The entrance section was 15.24-cm wide, and the main test section was divided by a partition into two passages 12.7-cm wide. One passage was open, and the other passage contained three rows of 0.95-cm diameter pins in a staggered array. These pins were spaced 2.54-cm apart laterally in rows also spaced 2.54-cm apart. This configuration captures the significant features of the cooled radial turbine blade shown in Fig. 3:<sup>1</sup> namely, the flow split created by a partition, the sharp corner, the cylindrical pins for turbulence generation, and leading-edge stagnation regions. Entrance velocities were measured by the differential between a wall static pressure tap and a total pressure probe at the entrance. Pressure, temperature, and flow data were recorded by a commercial data-acquisition system. Photographic data were taken with one or more video cameras.

For the heat transfer tests, a 0.025-mm thick Inconel sheet with a known uniform electrical resistance was attached to the floor of both the entrance and main test sections with a double-coated adhesive material. Each sheet had copper bus bars spot welded to it, was

coated with black lacquer, then spray painted with liquid crystals. A cross section of the test surface (Fig. 4) shows the 2.5-cm-thick foam insulation that prevented heat loss through the floor. For the heat transfer tests, the cylindrical pins were made of copper in order to simulate an actual blade where the surface heat is transferred to the pins. The pins were not attached to the surface but rested on the surface simply by gravity.

The test section for the flow visualization tests was identical in configuration to the heat transfer test section but without the liquid-crystal heater sheets and without the foam insulation. Another difference is that the pins were made of clear acrylic plastic instead of copper. This allowed the laser light sheet to partially pass through the pins to illuminate the flow field.

### Procedure

#### Liquid-Crystal Calibration

The liquid-crystal layer was calibrated for color-temperature correspondence by a thermocouple attached to each heated Inconel sheet. Dark blue corresponded to the highest temperature; blue, green, yellow, and reddish-brown corresponded to decreasing levels of temperature. Yellow occurred over the narrowest temperature band of 0.06 °C and was therefore the color used for temperature measurement. The yellow color location could be changed by varying the electrical heat input to the sheet under flow conditions. During calibration, when the yellow color was at the same location as the thermocouple, the temperature reading was 37.8 °C. This was, therefore, the calibration temperature.

#### Experimental Measurements

Entrance Velocity Profile and Turbulence Intensity. Velocity profiles were measured near the upstream end of the entrance test section by a surface static pressure tap and a traversable total pressure probe. As measurements were made, the probe was moved in small increments from the floor surface to a location just above the midchannel height position. It was physically impractical to measure the profiles at higher positions. Because the entrance passage was symmetrical about the midchannel height position, it was assumed that the velocity profile from midheight to the test section ceiling was identical to the measured profile from midheight to the floor. Free-stream turbulence intensity was measured by hot wire anemometry. All the measurements were made at entrance Reynolds numbers of approximately 45,000, 335,000, and 726,000.

Heat Transfer. Heat transfer tests were performed at the same entrance Reynolds numbers used for the

other measurements: 45,000, 335,000, and 726,000. These corresponded to a range of velocities from 9.14 to 155.5 m/sec. The operating procedure was initiated by bringing the tunnel to the velocity necessary to produce the desired Reynolds number. Electric power was then supplied to both entrance and main test section Inconel sheets at a matching heat flux, raising the temperature of the liquid crystal to the point at which color patterns appeared. The location of the yellow color lines was varied over the surface by changing the power input while the free-stream velocity remained the same. Between data recordings, typically about 15 min was given to allow thermal equilibrium to occur. Data were taken by four charged-couple device (CCD) color video cameras mounted high above the test section. One camera viewed the entire entrance section, another camera viewed the entire main test section, and the final two cameras gave closeup views of the cylindrical pin area. All four cameras were activated simultaneously to achieve time correspondence, and the data were recorded on Super VHS video tape. A photograph of the test section under flow conditions is shown in Fig. 5. The color-temperature patterns on the surface are clearly visible.

Flow Visualization. Flow visualization tests were performed at only one entrance Reynolds number, 45,000. In these tests, the flow was seeded with 1- $\mu$ m polystyrene spheres that followed the flow field. These particles were suspended in a heated water-ethyl alcohol mixture and sprayed into the flow stream with a spray nozzle. By the time the mixture reached the test section, much of the liquid had evaporated. The particles were illuminated by a 7-W argon-ion laser beam that was focused, through a series of mirrors and lenses, to a sheet of light approximately 2 mm thick. The result was a thin, illuminated, horizontal slice of the flow field at midchannel height.

A single black and white CCD video camera recorded the flow, showing the trajectories of the particles as streaklines on each video frame. A light chopper was placed in the laser beam to measure the velocity of the flow field. This chopper, which consisted of a rotating disk with holes spaced such that the light was periodically blocked, could chop light at a maximum frequency of 3000 Hz. The instantaneous velocity of the particles was represented by the distance between interruptions in the streaklines on any one video frame as illustrated in Fig. 6. Similarly, the acceleration of the particles was represented by the change in the distance between interruptions in the streaks. Because of the high magnification required to see the particle traces, only one small area could be viewed at a time. A computer-aided design (CAD) software package was used to combine the data from approximately 300 individual frames so that all of the information could be presented in one composite picture.

## Data Reduction

Heat Transfer. Surface heat transfer coefficients were calculated as follows:

$$h = \frac{Q_e - Q_L}{A(T_{LC} - T_R)}$$

The local heat transfer coefficient  $h$  was calculated at the location of the calibrated color band (an isotherm—which in this case also represents a uniform heat transfer coefficient). The heat energy  $Q_e$  supplied to the heater sheet was calculated from the measured voltage across the sheet and the current through a shunt resistor in series with the sheet. The heat loss  $Q_L$  was the calculated radiation from the surface. The insulation under the test cell floor prevented back side heat loss, and other heat losses were considered negligible. The area  $A$  was the measured area of the Inconel heater sheet, and the temperature of the test surface  $T_{LC}$  was the calibrated liquid-crystal temperature. The recovery temperature  $T_R$  of the entrance free-stream air was calculated as

$$T_R = T_s + r(T_t - T_s)$$

where  $T_s$  and  $T_t$  are the static and total air temperatures, respectively, and  $r$  is the recovery factor, defined as the cube root of the Prandtl number.

An uncertainty analysis based on the method described in Refs. 8 and 9 was performed on the calculation of experimental heat transfer coefficients. With this method, the maximum expected uncertainty values in the calculation of heat transfer coefficients were 14.0, 3.7, and 3.8 percent for Reynolds numbers of 45,000, 335,000, and 726,000, respectively. The relatively high percentage heat transfer uncertainty at the lowest Reynolds number resulted from a high uncertainty in flow velocity because of the lower accuracy of the pressure-measuring devices at very small pressure differentials. At all Reynolds numbers, errors were also possible in reading the exact location of the isotherms.

The heat transfer video data were reduced with a personal computer equipped with a commercial video frame grabbing board. A computer program was written to manually digitize (trace) the yellow color bands from a video image grabbed from the video tape, and the digitized image was stored in a computer. The digitized locations along with the measurements of surface heat flux, air temperature, and free-stream velocity allowed the calculation of heat transfer coefficients.

Flow Visualization. The method for reducing the flow visualization data is described in detail in Ref. 7. In the present study, the region of the test section mapped with this technique was greatly increased to include an area from 8.9-cm upstream of the front row of pins to 3.8-cm downstream of the last row of pins.

The uncertainty involved in determining velocity is largely dependent on the accuracy of the operator during the digitizing process. Reference 7 reports that maximum expected errors may vary from 4 to 8 percent.

## Computational Solutions

Computational solutions of the flow field and heat transfer coefficients along the floor of the test section were obtained with the commercially available code, STAR-CD.<sup>10,11</sup> This code solves the fully three-dimensional, turbulent compressible Navier-Stokes equations on an unstructured mesh with local mesh refinement capabilities. The governing equations of mass, momentum, energy, turbulent kinetic energy, and dissipation are discretized by the finite volume method, and a semi-implicit formulation is utilized (SIMPLE scheme).<sup>12</sup>

The computational mesh for this analysis is shown in Fig. 7. Because computer resources were limited, the computational grid was limited to about 250,000 cells, with finer mesh generated in the pin region. Boundary conditions were set at the entrance plane and at the exit of the computational domain to match those of the experimental values at Reynolds numbers of 45,000, 335,000, and 726,000. Because of difficulties encountered trying to input the measured velocity profile into the code, a constant velocity profile was used at the entrance. This profile was the free-stream velocity measured at the entrance plane of the test section. In addition, the average experimentally measured turbulence level of 2.3 percent was specified. A constant pressure was assigned at the exit, and the walls were specified to be at a constant temperature.

Steady-state calculations with the upwind difference scheme were chosen for this analysis. The  $k-\epsilon$  turbulence model was used, and heat transfer coefficients were obtained with the Reynolds analogy, which relates the convective heat transfer coefficient to the shear stress of the flow at the wall. A Unix-based, Silicon Graphics' Iris workstation with four central processing units (cpu's) in parallel was used to run the analysis and to pre- and post-process the data. The cpu time for obtaining a convergent solution ranged from 29 to 55 hr.

The converged solution of the flow provided velocities, pressures, temperatures, density variations, and various other parameters throughout the channel, as well as heat transfer coefficients on the surface.

## Results and Discussion

### Experimental Results

**Entrance Velocity Profiles.** Velocity profiles at the entrance are shown in Fig. 8 for the three entrance Reynolds numbers of 45,000, 335,000, and 726,000. Fully developed flow had not occurred, and as expected, there was a slight decrease in boundary-layer thickness as velocity was increased. The boundary-layer thickness, defined as the point where the velocity is 99 percent of the free-stream value, was 1.55 cm at a Reynolds number of 45,000, 1.40 cm at 335,000, and 0.94 cm at 726,000.

The velocity data were also plotted logarithmically in terms of dimensionless coordinates (Fig. 9). This plot was made to show how the boundary layer compared with turbulent boundary layers normally encountered in turbine flow. Included in the figure is the calculated theoretical line for a fully turbulent boundary layer. The equations used were taken from Ref. 13. The experimental data match the theoretical line fairly well.

**Free-Stream Turbulence Intensity.** Free-stream turbulence intensity was measured with a hot wire anemometer at midchannel height. At a Reynolds number of 45,000 the turbulence intensity was measured as 2.8 percent, at a Reynolds number of 335,000 it was 1.2 percent, and at a Reynolds number of 726,000 it was 2.9 percent. The average intensity was 2.3 percent. It has not been determined why the turbulence intensity was so much lower at the medium value of Reynolds number.

**Heat Transfer Measurements.** Quantitative heat transfer coefficients on the floor of the test section were mapped for three different entrance Reynolds numbers. A typical example of the results is shown in Fig. 10. Parts (a) to (c) are actual video screen photographs of the surface at the lowest Reynolds number of 45,000 and at three of the various electrical energy inputs. The figure includes closeup views of the color-temperature patterns around the pins. Figure 11(a) shows the corresponding map of heat transfer coefficients calculated from these isotherms, and Fig. 11(b) is a closeup of the area around the pins. Similar heat transfer maps are shown in Figs. 12 and 13 for Reynolds numbers of 335,000 and 726,000, respectively.

Generally, the heat transfer patterns were similar for all Reynolds numbers. The heat transfer in the

entrance region decreased going downstream as shown in Figs. 11(a), 12(a), and 13(a). Areas of low heat transfer are seen in the front left (relative to the flow stream) corner of the main test section where the flow is recirculating. The lowest values of heat transfer occurred in this region at all three flow conditions as shown in these same figures. In the unobstructed passage (no pins) there is a similarity in the pattern of the heat transfer at all three flow conditions with a high value heat transfer coefficient coming off the partition leading edge (probably produced by the accelerating flow and high turbulence created in this area, as will be discussed later). The heat transfer coefficients decreased as flow progressed downstream. Close to the partition, the coefficients were even smaller, probably because of a flow separation in this area. From the closeup views of the pin region (Figs. 11(b), 12(b), and 13(b)), the cooling effectiveness of the pins is evident by the color patterns immediately downstream of the pins and the corresponding high values of heat transfer coefficients. Further downstream of the pins, the heat transfer coefficients decreased. At some locations, the experimental contours were broad bands instead of thin lines, indicating very gradual surface temperature gradients.

**Flow Field Measurements.** Flow field measurements were made at an entrance velocity of 9.14 m/sec, which corresponded to the lowest Reynolds number of 45,000. Attempts were made to obtain results at the higher Reynolds numbers, but these attempts were unsuccessful with the equipment that was available. As the velocity of the flow field was increased, it was more difficult to detect individual traces on the video screen. The maximum measurable particle velocity was further limited by the maximum frequency at which the light chopper could operate, which was 3000 Hz. As previously shown (Fig. 6), the velocity was determined by the distance between interruptions in the streaks shown in any one video frame. At higher velocities, streaks would appear in a single frame with either one interruption or no interruptions at all, making it impossible to determine the velocities or accelerations.

Figure 14(a) is a video picture of the particles as they flowed between a pin and the partition leading edge. Figure 14(b) shows the data after being processed into velocity vectors. The numbers on the diagram identify each particular trajectory, and the magnitude of the velocity is indicated by the length of the arrows.

Figure 15 is a composite view of about 300 video frames, giving an overall view of the flow field in the area investigated. Velocity vector diagrams similar to the one shown in Fig. 14(b) can be generated anywhere within this area from the data collected in this study. Figure 15 reveals a few features that help explain some of the heat transfer results. A turbulent area appears

immediately downstream of the pins, which corresponds to the high heat transfer area seen in the maps. In the unobstructed passage where the flow comes off the partition, there seems to be a region of turbulent flow bordered by an area of smooth accelerated flow. This corresponds to the high values of heat transfer seen on the heat transfer maps. In the front left corner of the main test section, the flow mapping appears to indicate a highly turbulent, high velocity area; but actual observation of the flow showed this area to have very slow, three-dimensional flow, making it difficult to properly visualize the flow in a thin slice of light. The seeded air seemed to just circle slowly around in a lazy manner, which would lead to the low heat transfer and high surface temperatures indicated in the heat transfer tests.

### Computational Results

Heat Transfer Computations. Computational solutions for the surface heat transfer coefficients were obtained for all three Reynolds numbers. The results are shown in Fig. 16 for a Reynolds number of 335,000 for comparison with the experimental results. Figure 16(a) shows a decreasing value of heat transfer coefficient in the entrance section. Low values were seen in the recirculation region as expected. In the area downstream of the pins, the isotherms occurred in a generally longitudinal direction. Figure 16(b) shows a closeup view of the area around the pins. Low values were calculated in the wake of the pins.

Flow Field Computations. Computational solutions for velocities at midchannel height of the flow field are shown in Fig. 17. The color chart designates the magnitude of the velocities. These solutions were obtained for a Reynolds number of 45,000, which corresponds to an entrance velocity of 9.14 m/sec. As the flow approached the pins and the partition area, it accelerated into the unobstructed passage, whereas the flow going through the pins decelerated. The recirculation region shows very low velocities in the range of 2 to 4 m/sec. The flow in the pin area does not seem to be as turbulent as expected. Evidently, the grid around the pins was not fine enough to show the complex mixing that occurs in the wake regions.

### Computational-Experimental Comparisons

Heat Transfer Comparisons. There is agreement in some of the general trends between the experimental and computational results (for example, the decreasing heat transfer in the entrance region), but there is disagreement in the numerical values around and downstream of the pins. Because the Reynolds analogy was used in the analysis, this calculation would not be expected to be valid around the pins. In addition, the computational map, which shows longitudinal, fingerlike contours

downstream of the pins, differs from the experimental maps, which showed almost constant heat transfer lines across the channel. Figure 16 shows high heat transfer coefficient values in the high acceleration region between the partition and the recirculation area, whereas Figs. 11 to 14 show high heat transfer coefficient values in the high turbulent flow coming off the partition. The use of a finer mesh grid near the floor, where the heat transfer is calculated, might have produced more compatible results. In the recirculation region, the calculation shows a low heat transfer coefficient, which is confirmed by the experiment.

Flow Field Comparisons. Because experimental flow field data were obtained at only one entrance flow velocity, 9.14 m/sec, a comparison between computational and experimental results could be made only at the one corresponding Reynolds number of 45,000 and only at one small area at a time. The area chosen was the region near the leading edge of the partition and the nearest pin. A close-up view of the flow in this area is shown in Fig. 18. (This view is at midchannel height.) In the area upstream of the pins, there is good agreement with experimental velocities at about 7.5 m/sec. However, in the area between the partition and the pin, the code showed the flow decelerating to 5.5 m/sec, which is lower than experimental values seen in Fig. 14(b). The calculated values for the flow field show the general trends, but failed to predict the levels and details around the pins. The grid that was used to compute the flow field around the pins consisted of 16 cells around the pins and 20 cells deep—evenly spaced from top to the bottom of the channel. The number of the grid points was chosen arbitrarily to maintain a reasonable size grid and to obtain a solution in a timely manner. Using a denser grid or assuming symmetry about the midchannel height and analyzing only the lower half with the same number of grid points might have generated a better flow field calculation. Such refinements will be attempted at a later date.

### Concluding Remarks

The experimental investigation revealed the temperature patterns that occur throughout a test section with some significant features of an internal passage of a cooled turbine blade. Areas of high and low heat transfer were identified, and quantitative heat transfer data were obtained over a range of flow conditions. The cooling effectiveness of the cylindrical pins was demonstrated. Areas of recirculating and separating flows and their effect on surface temperature patterns were evident. The experimental flow visualization data generally supported the heat transfer data in terms of explaining some of the temperature patterns. Two benchmark sets of data were produced, heat transfer and flow field,

which are now available for internal cooling code validation.

Computational solutions for the flow field and surface heat transfer were obtained with a commercially available code, STAR-CD. These solutions showed general trends of the flow field in the channel. The magnitude of the velocity field around the pins was lower than the experimental values. The code-predicted heat transfer results agreed with some of the general trends of the experimental data, but there were differences in the numerical values of the surface heat transfer coefficients on most of the channel floor. In the pin area, the calculated heat transfer coefficients downstream of the pins showed trends opposite to those of the experiment. The grid size of 250,000 cells was evidently insufficient to resolve the flow field in this area as well as the heat transfer.

STAR-CD, which is typical of currently available, general purpose, computational fluid dynamics (CFD) codes, showed the limitations that exist at the present time in predicting the flow field and heat transfer in complex geometries. The difficulties encountered in attempting to match computational simulation and experimental data demonstrate the need for further development of CFD codes.

#### References

1. Snyder, P.H., and Roelke, R.J., "The Design of an Air Cooled Metallic High Temperature Radial Turbine," AIAA Paper 88-2872, July 1988.
2. Becker, W.J., and Steiner, A.L. "The Application of 3D Navier-Stokes Codes to Turbine Internal Cooling Problems," AIAA Paper 90-2267, 1990.
3. Steinthorsson, E., Shih, T.I.-P., and Roelke, R.J., "Computations of the Three-Dimensional Flow and Heat Transfer Within a Coolant Passage of a Radial Turbine Blade," AIAA Paper 91-2238, 1991.
4. Simoneau, R.J., and Simon, F.S., "Progress Toward Understanding and Predicting Convection Heat Transfer in the Turbine Gas Path," NASA TM-105674, 1992.
5. Prakash, C., and Zerkle, R., "Prediction of Turbulent Flow and Heat Transfer in a Radially Rotating Square Duct," Journal of Turbomachinery, Vol. 114, Oct. 1992, pp. 835-846.
6. Hippensteele, S.A., and Russell, L.M., "High-Resolution Liquid-Crystal Heat Transfer Measurements on the End Wall of a Turbine Passage With Variations in Reynolds Number," NASA TM-100827, 1988.
7. Braun, M.J., Canacci, V.A., and Russell, L.M., "Full Field Flow Visualization and Computer-Aided Velocity Measurements in a Bank of Cylinders in a Wind Tunnel," Experiments in Fluids, Vol. 13, No. 2-3, 1992, pp. 117-127.
8. Abernethy, R.B., and Benedict, R.P., "Measurement Uncertainty: A Standard Methodology," Proceedings of the 30th International Instrumentation Symposium, ISA, Research Triangle Park, NC, 1984, pp. 411-420.
9. Kline, S.J., and McClintock, F.A., "Describing Uncertainties in Single-Sample Experiments," Mechanical Engineering, Vol. 75, No. 1, Jan. 1953, p. 38.
10. Ippolito, J., and MacDonald, P.S., "Three-Dimensional Flow Analysis of the Internal Passage of a Cooled Radial Rotor." ADAPCO Report No. 30-02-004, Analysis and Design Applications Co., Melville, NY, Apr. 26, 1991.
11. "Star-CD Version 2.11 Users Guide," Computational Dynamics Limited, Melville, NY, 1991.
12. Patankar, S.V., Numerical Heat Transfer and Fluid Flow, McGraw Hill, New York, 1980.
13. Kays, W.M., Convective Heat and Mass Transfer, McGraw Hill, New York, 1966.

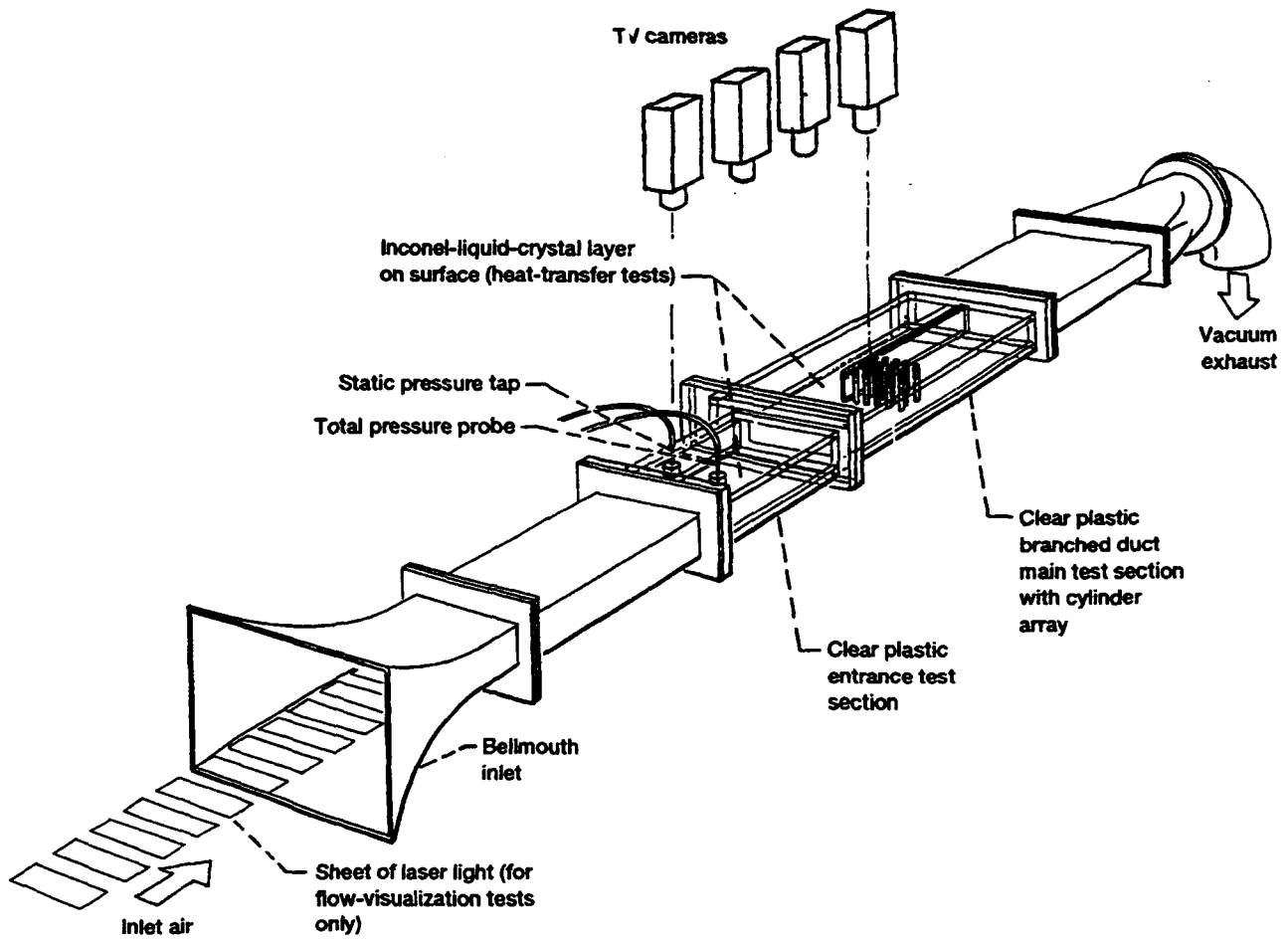


Figure 1.—Branched duct tunnel. Note: Only one camera used for flow-visualization tests.

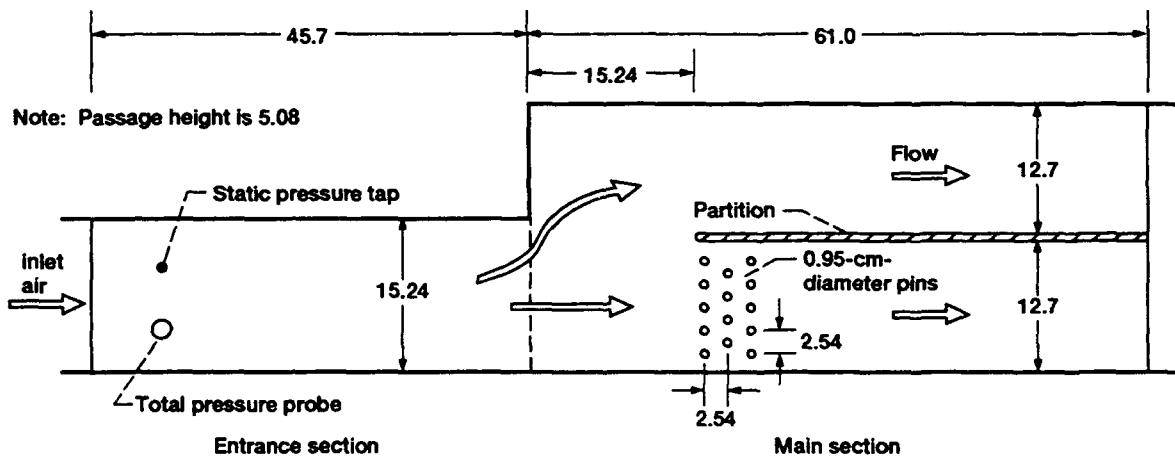


Figure 2.—Test section. (All dimensions given in centimeters.)

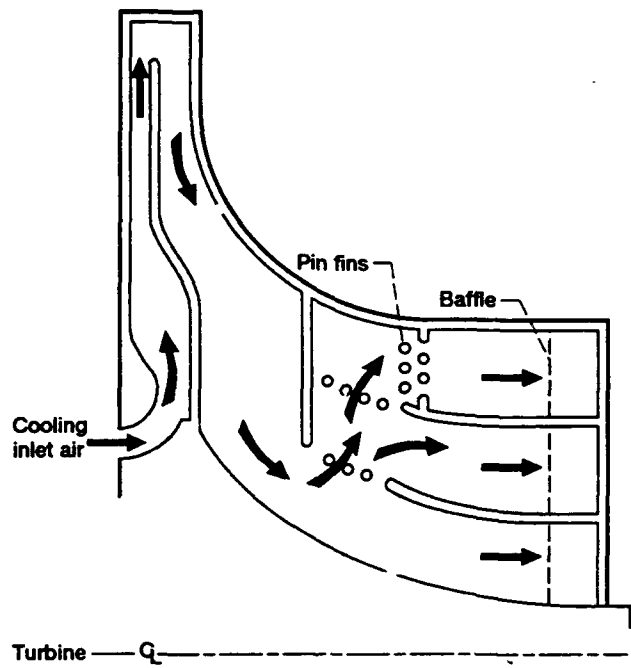


Figure 3.—Cooled radial turbine blade (Ref. 1).

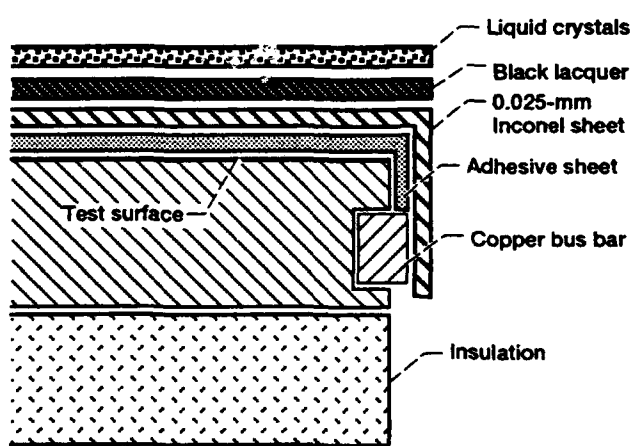


Figure 4.—Cross section of test surface.

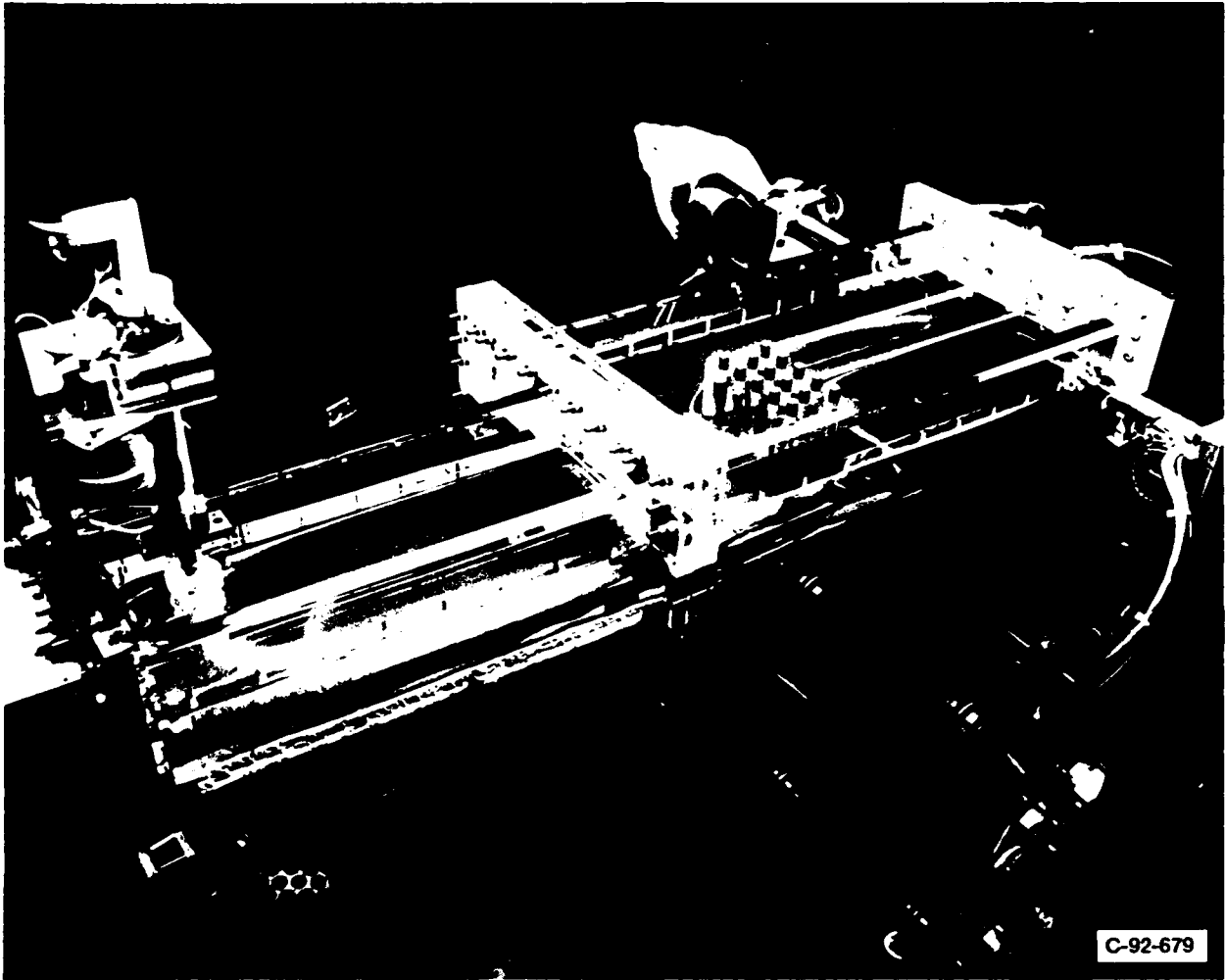


Figure 5.—Test section under flow conditions; Reynolds number, 45,000.

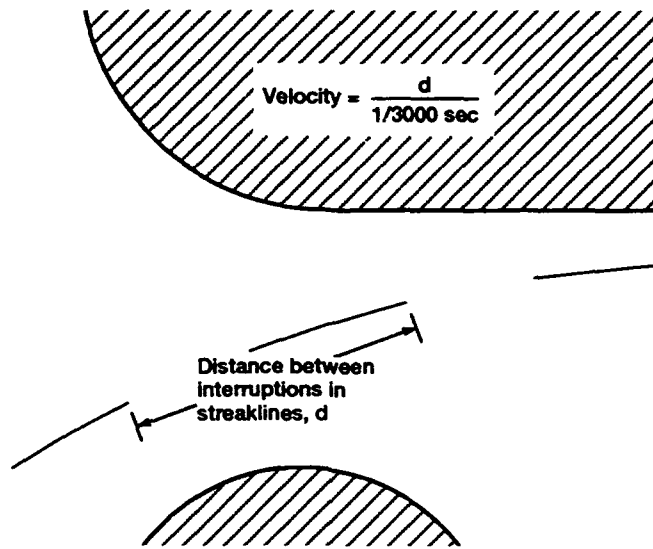


Figure 6.—Instantaneous velocity from 1/30-sec video frame using 3000-Hz light chopper.

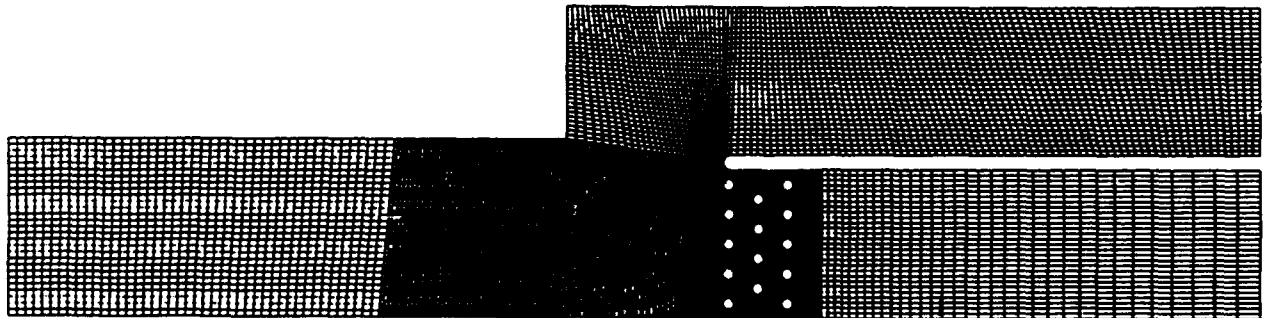


Figure 7.—Computational mesh.

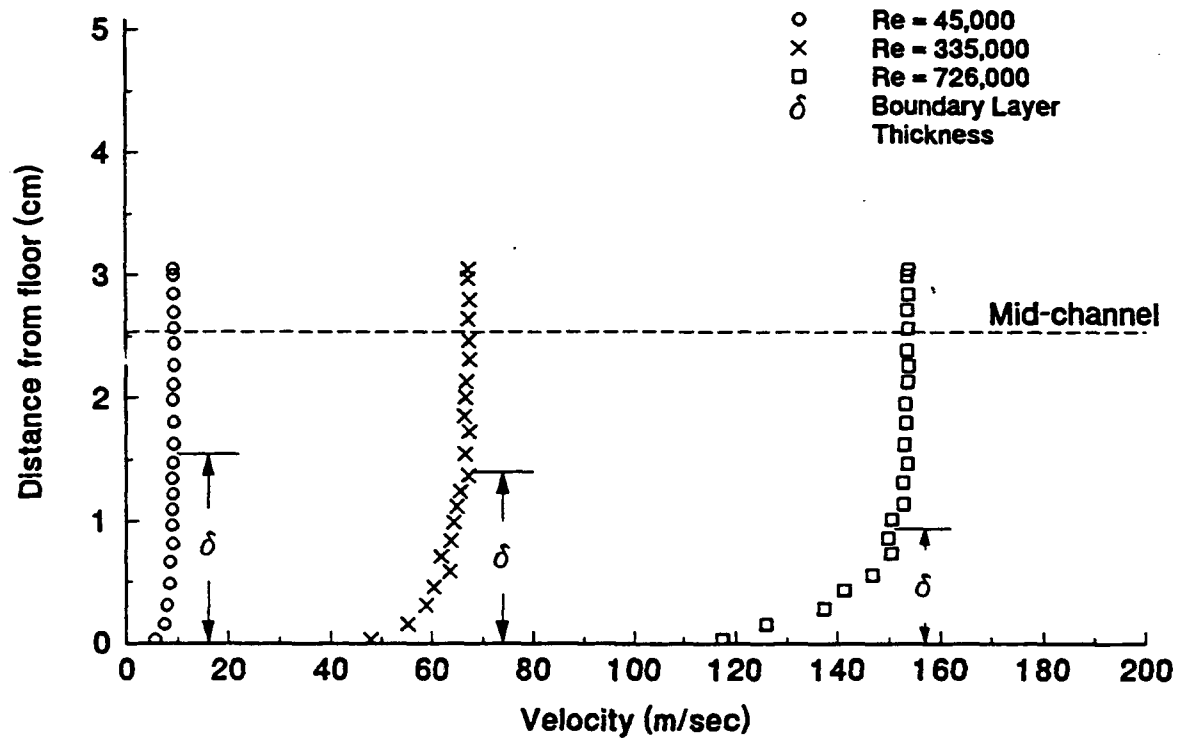


Figure 8.—Entrance velocity profiles.

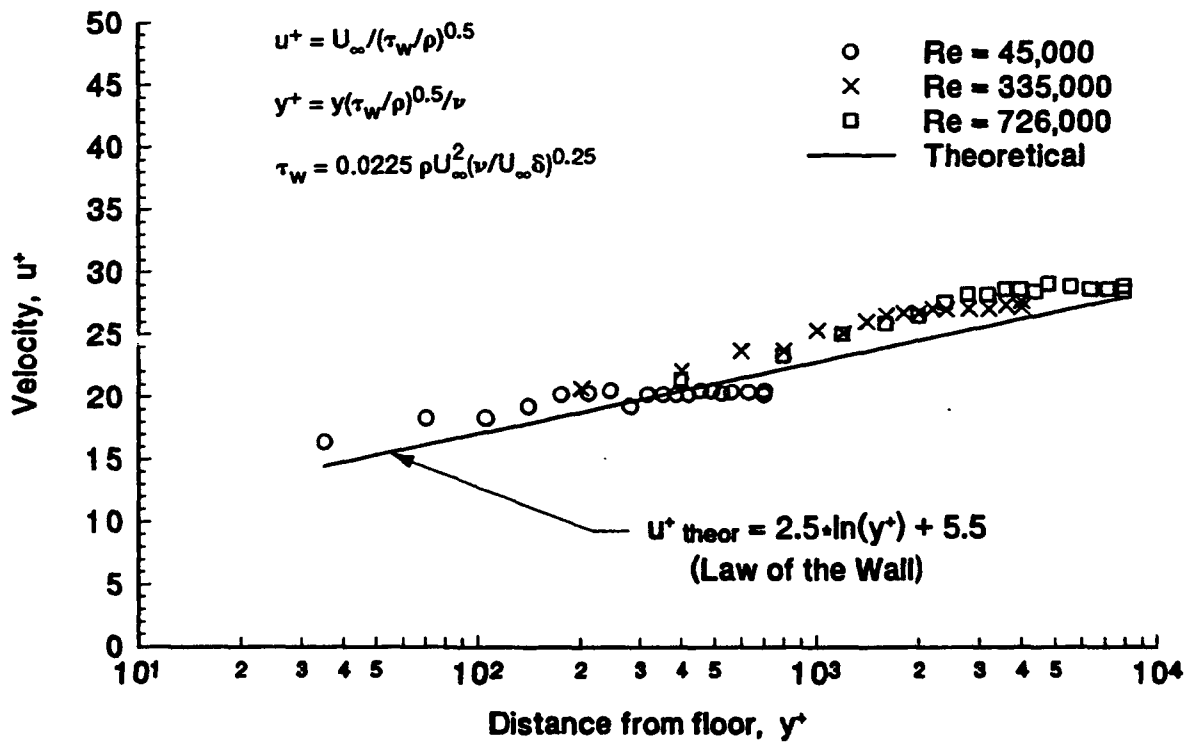
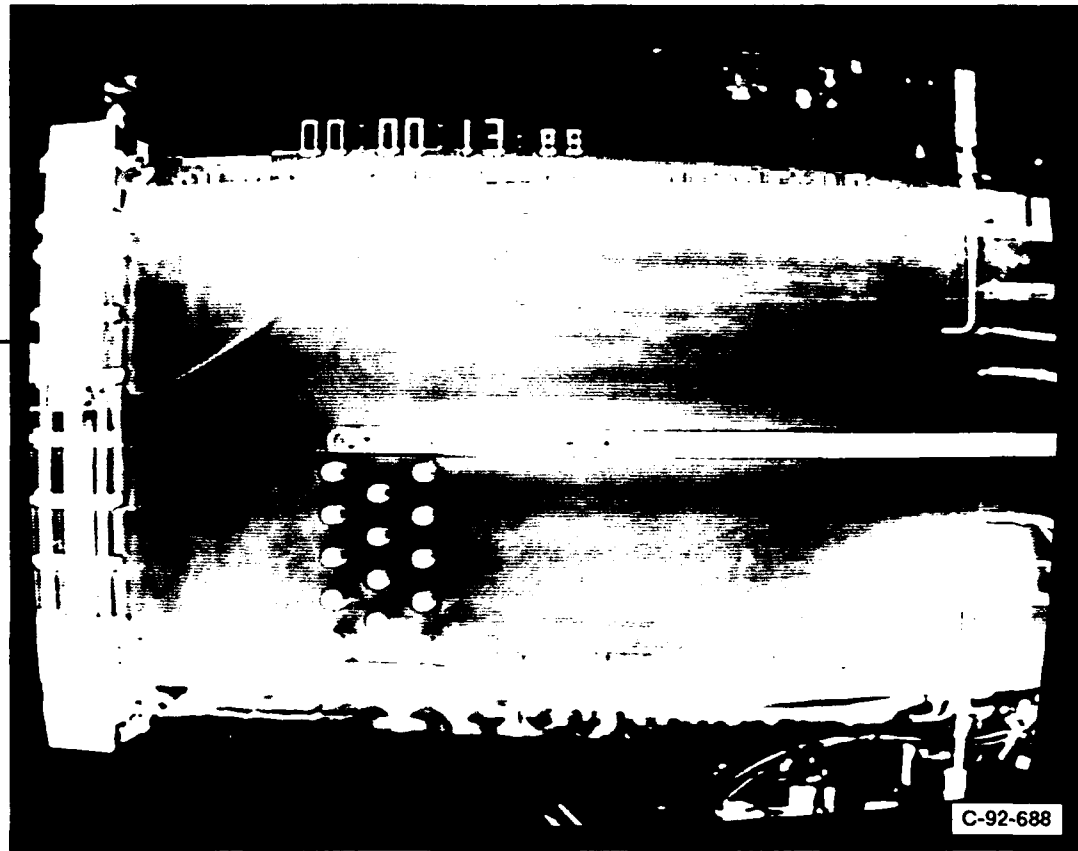


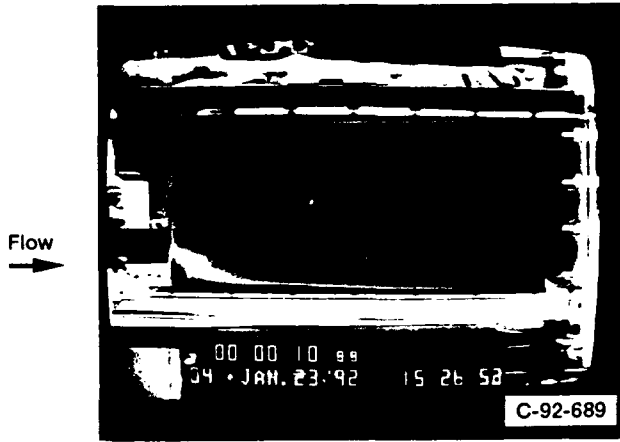
Figure 9.—Dimensionless boundary-layer profile.

Recirculation  
region

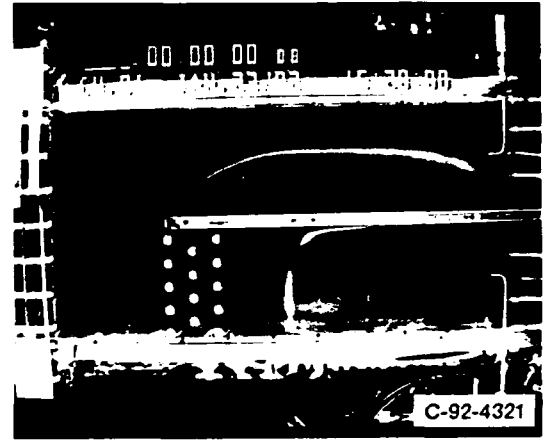


(a) Low-heat input; main section.

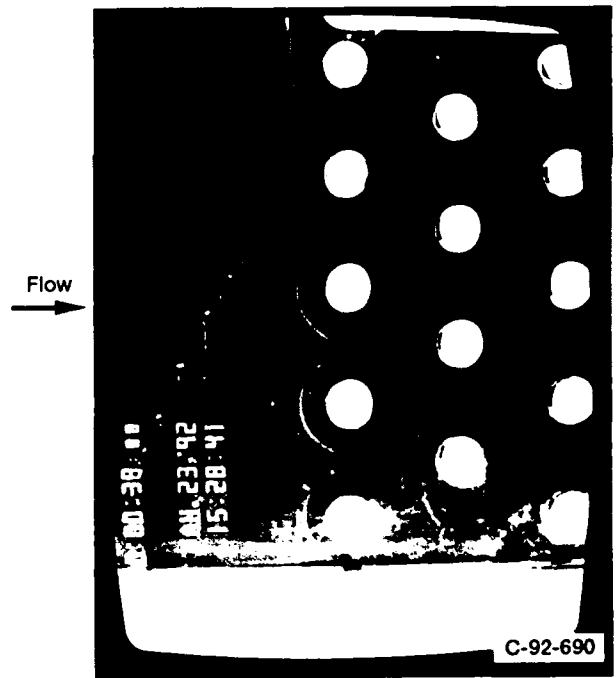
Figure 10.—Surface color-temperature patterns; Reynolds number 45,000.



Entrance section



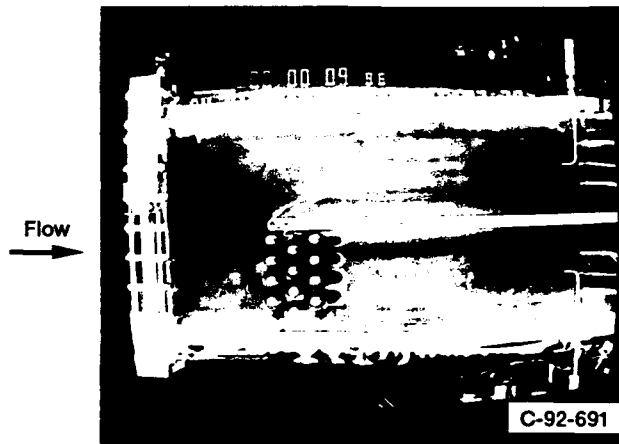
Main section



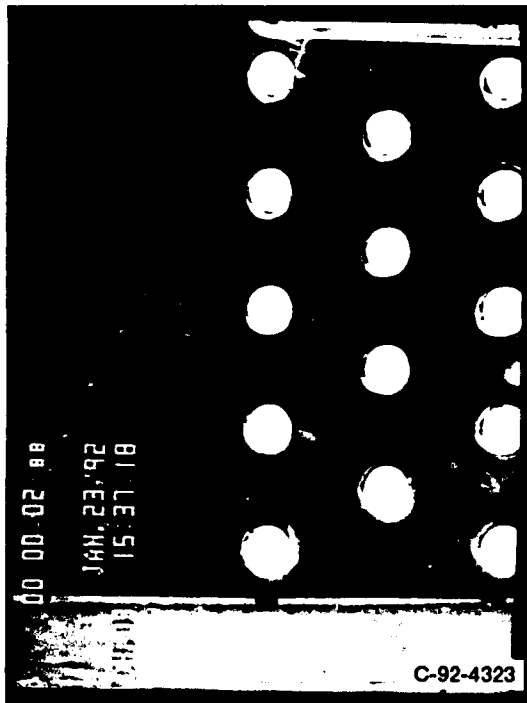
Close-up of pin area

(b) Medium heat input.

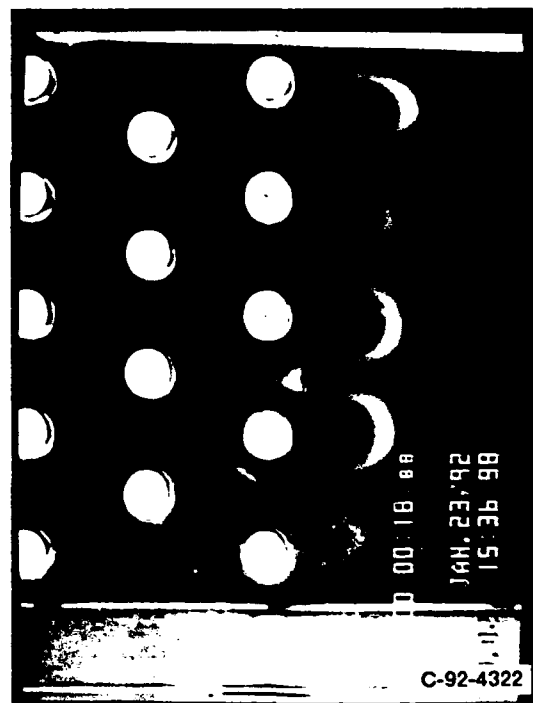
Figure 10.—Continued.



Main section



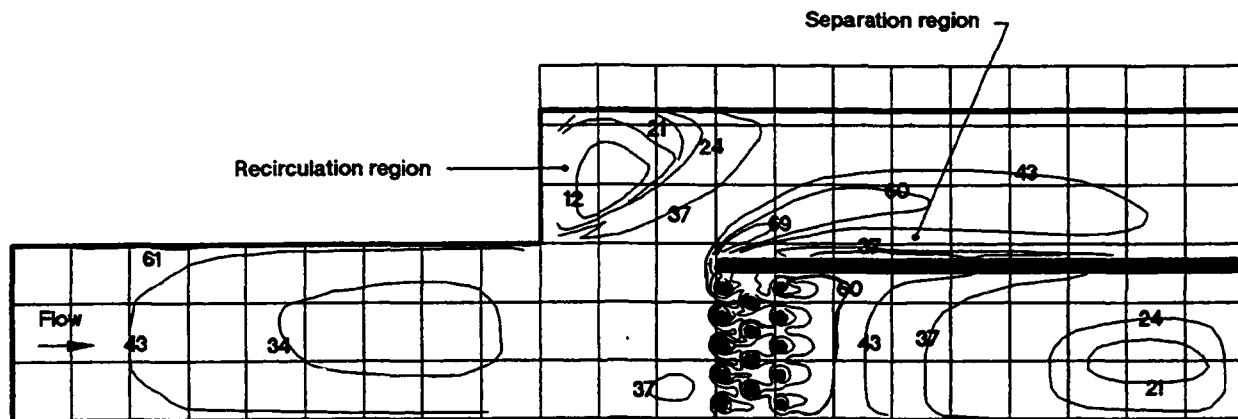
Close-up of pin array, upstream area



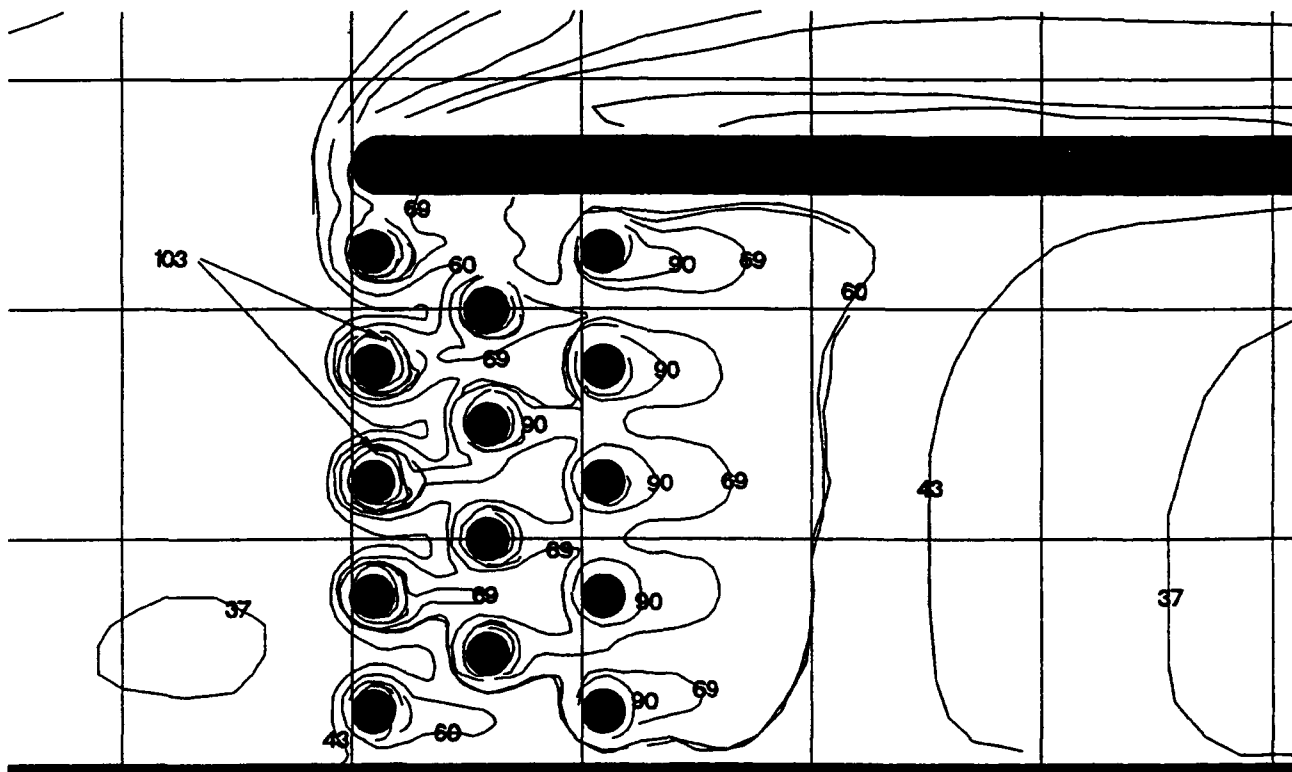
Close-up of pin array, downstream area

(c) High heat input.

Figure 10.—Concluded.

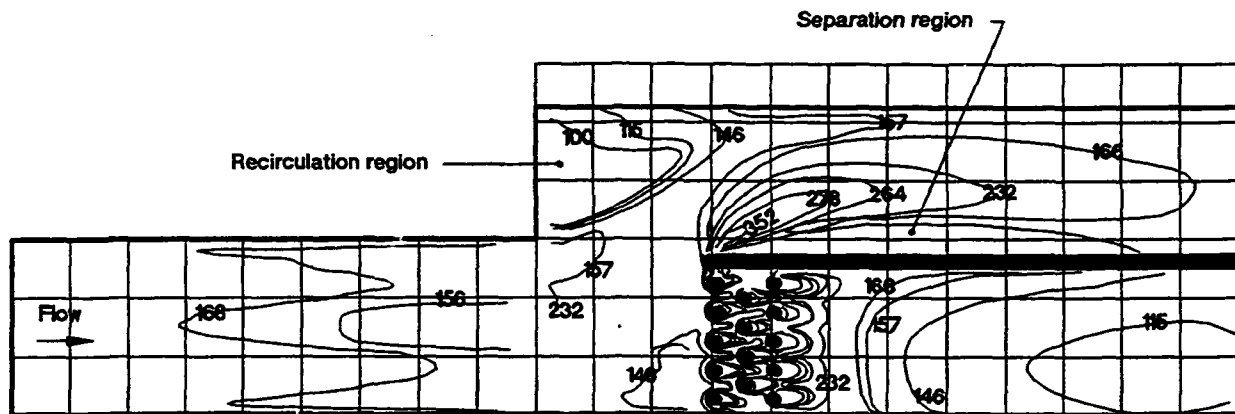


(a) Entire test surface.

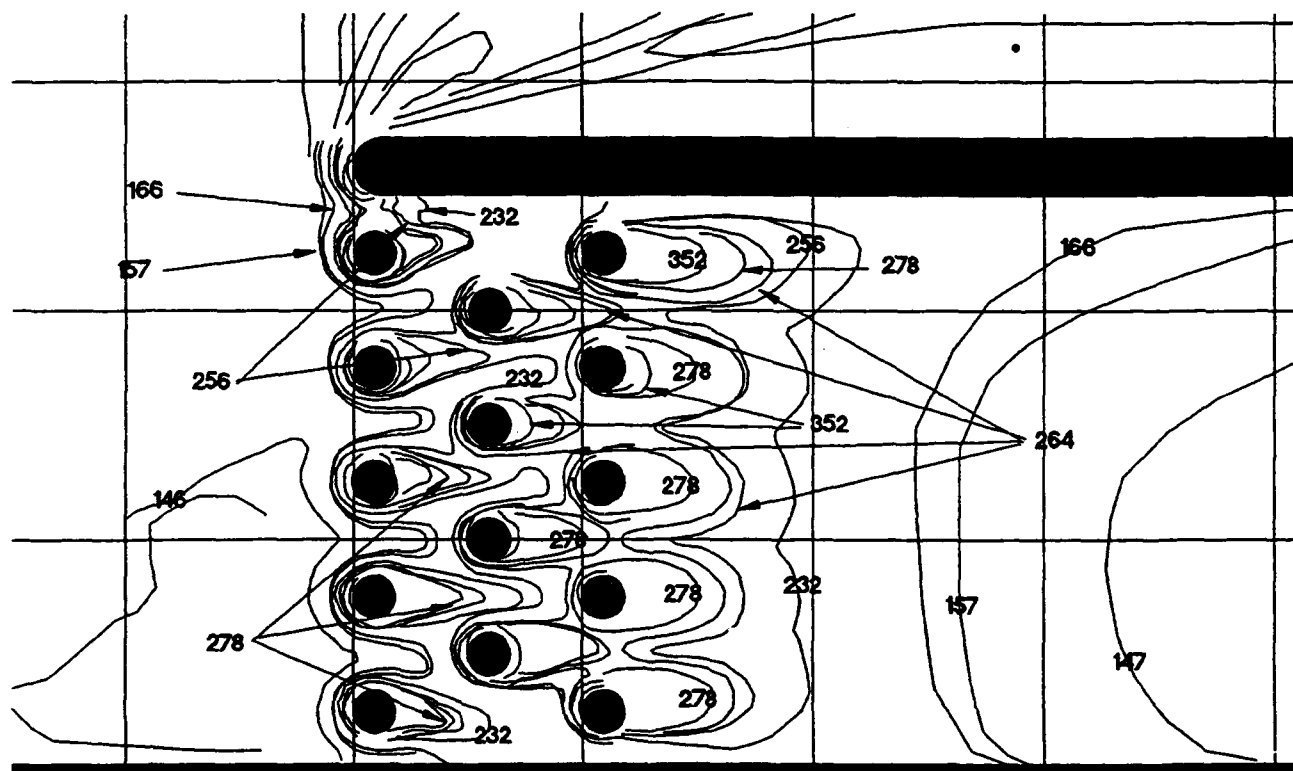


(b) Close-up of pin area.

Figure 11.—Experimental heat transfer coefficients; Reynolds number, 45,000. (Coefficients given in  $W/m^2 \cdot K$ .)

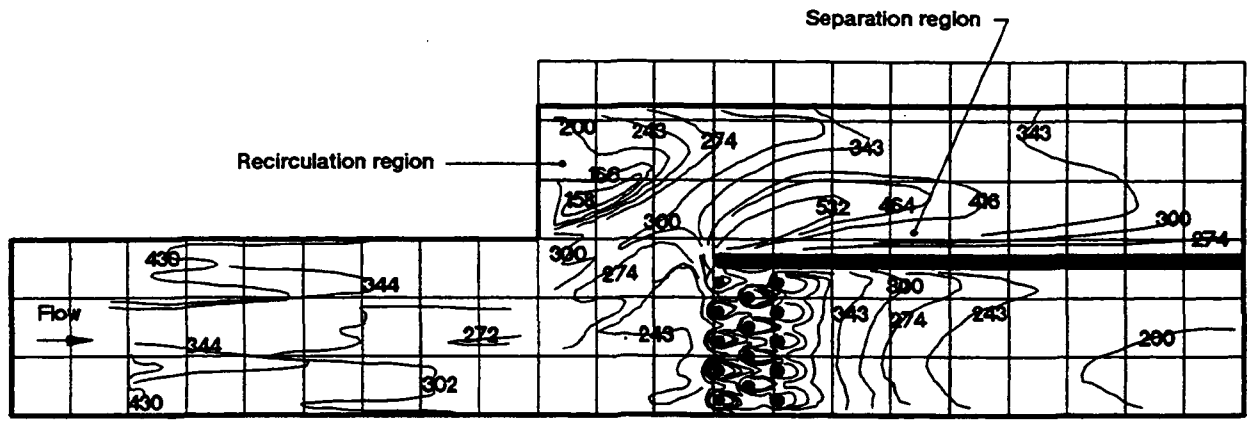


(a) Entire test surface.

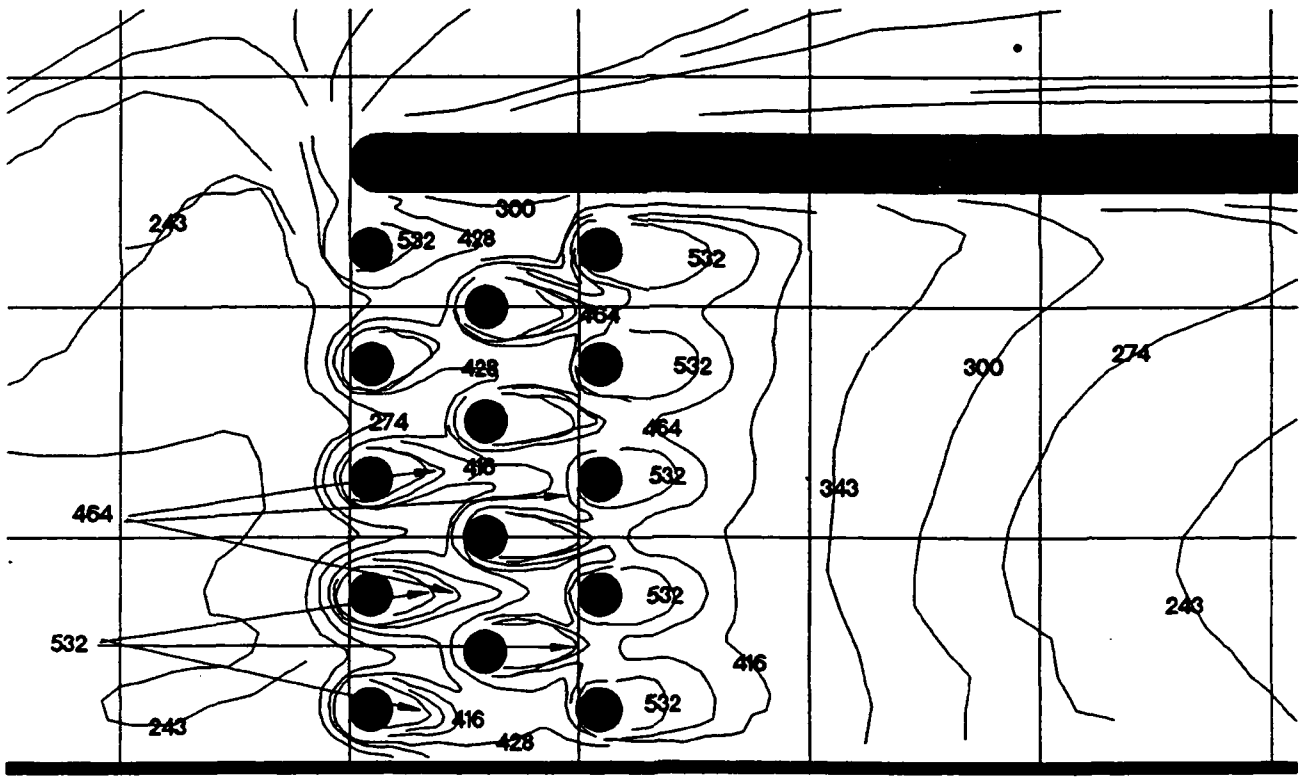


(b) Close-up of pin area.

Figure 12.—Experimental heat transfer coefficients; Reynolds number, 335,000. (Coefficients given in  $W/m^2 \cdot K$ .)



(a) Entire test surface.

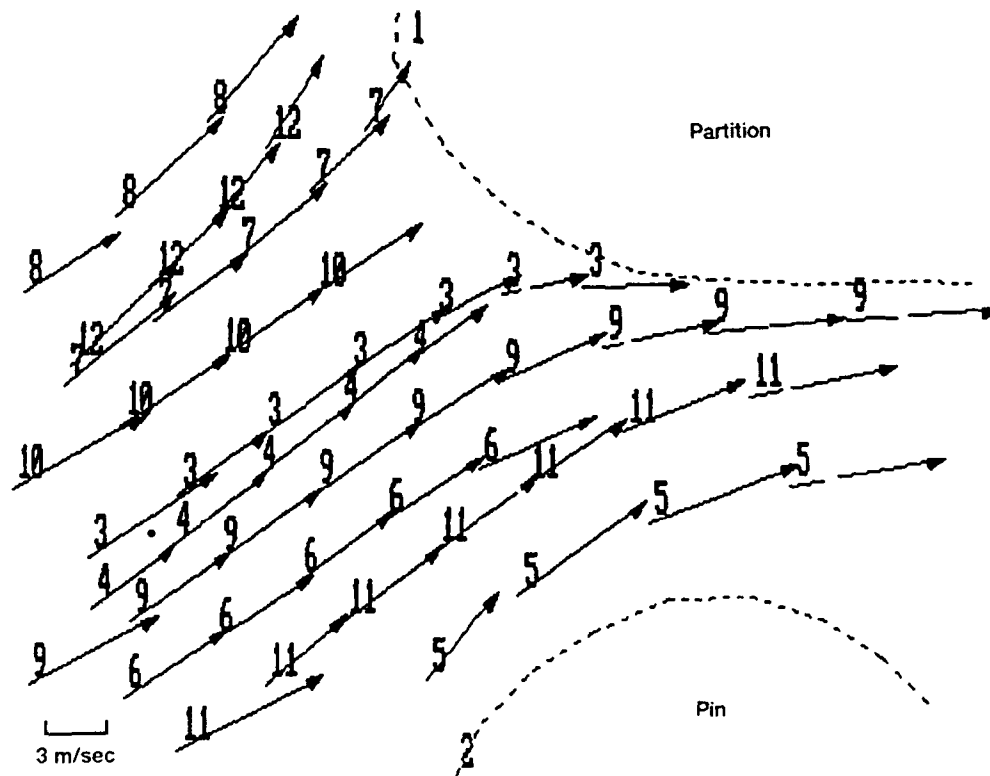


(b) Close-up of pin area.

Figure 13.—Experimental heat transfer coefficients; Reynolds number, 726,000. (Coefficients given in  $W/m^2 \cdot K$ .)



(a) Video picture.



(b) Velocity vector diagram.

Figure 14.—Particle trajectories; Reynolds number, 45,000.

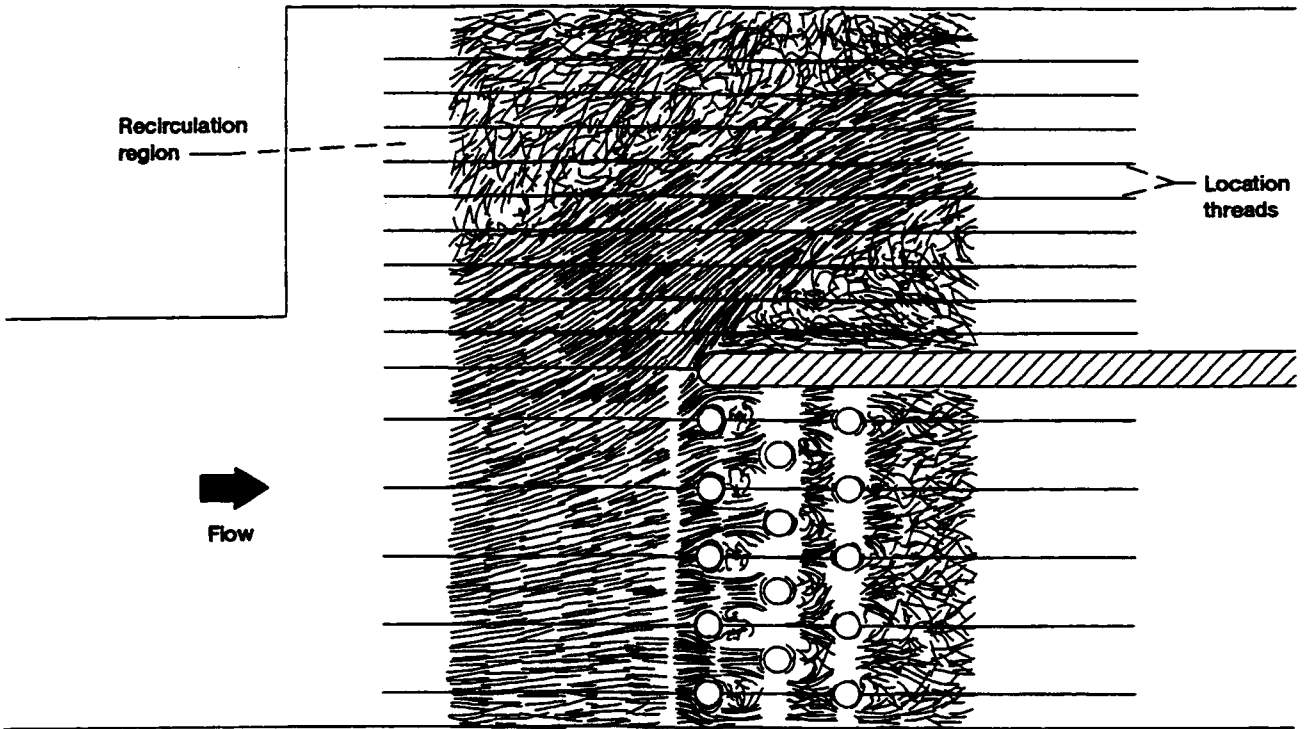
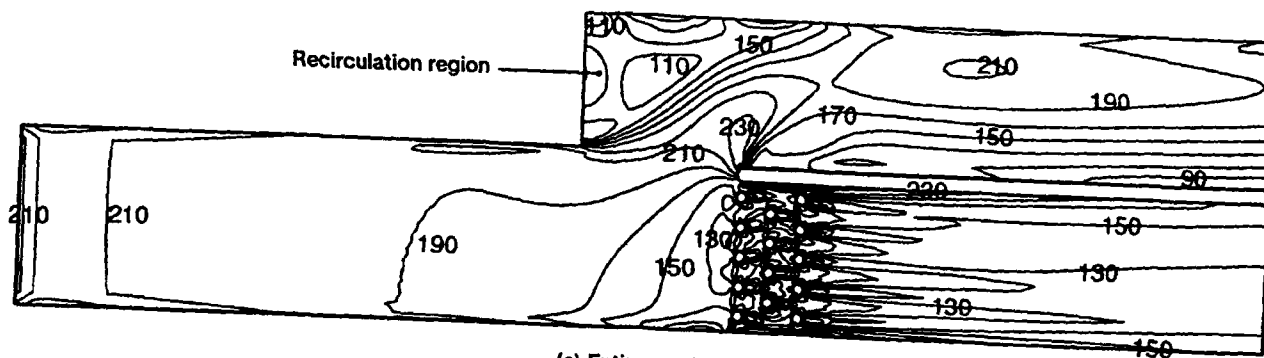
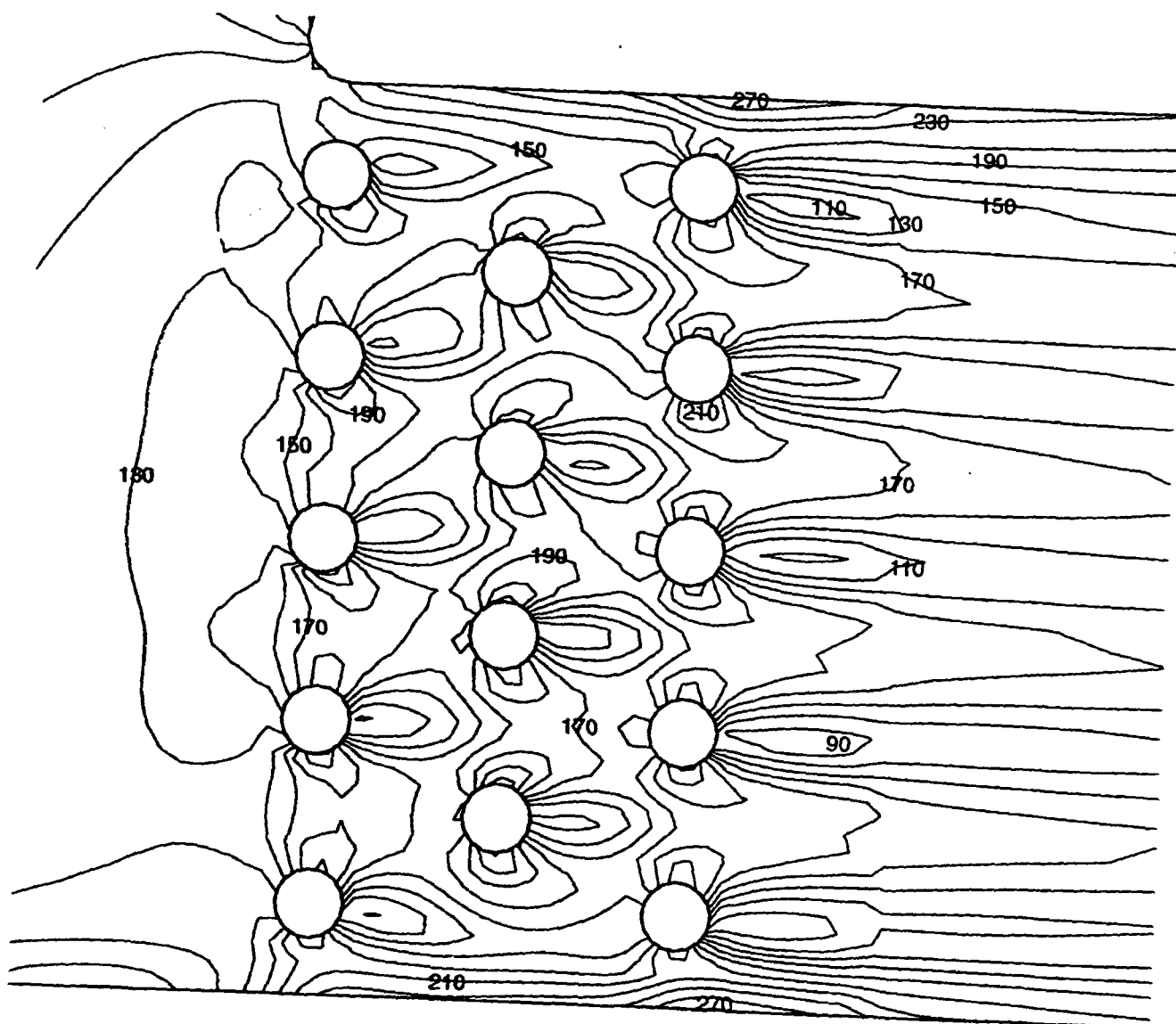


Figure 15.—Composite of digitized video data; Reynolds number, 45,000. (300 video frames combined.)



(a) Entire mesh.



(b) Pin area.

Figure 16.—Computational heat transfer coefficients; Reynolds number, 335,000. (Coefficients given in  $W/m^2 \cdot K$ .)

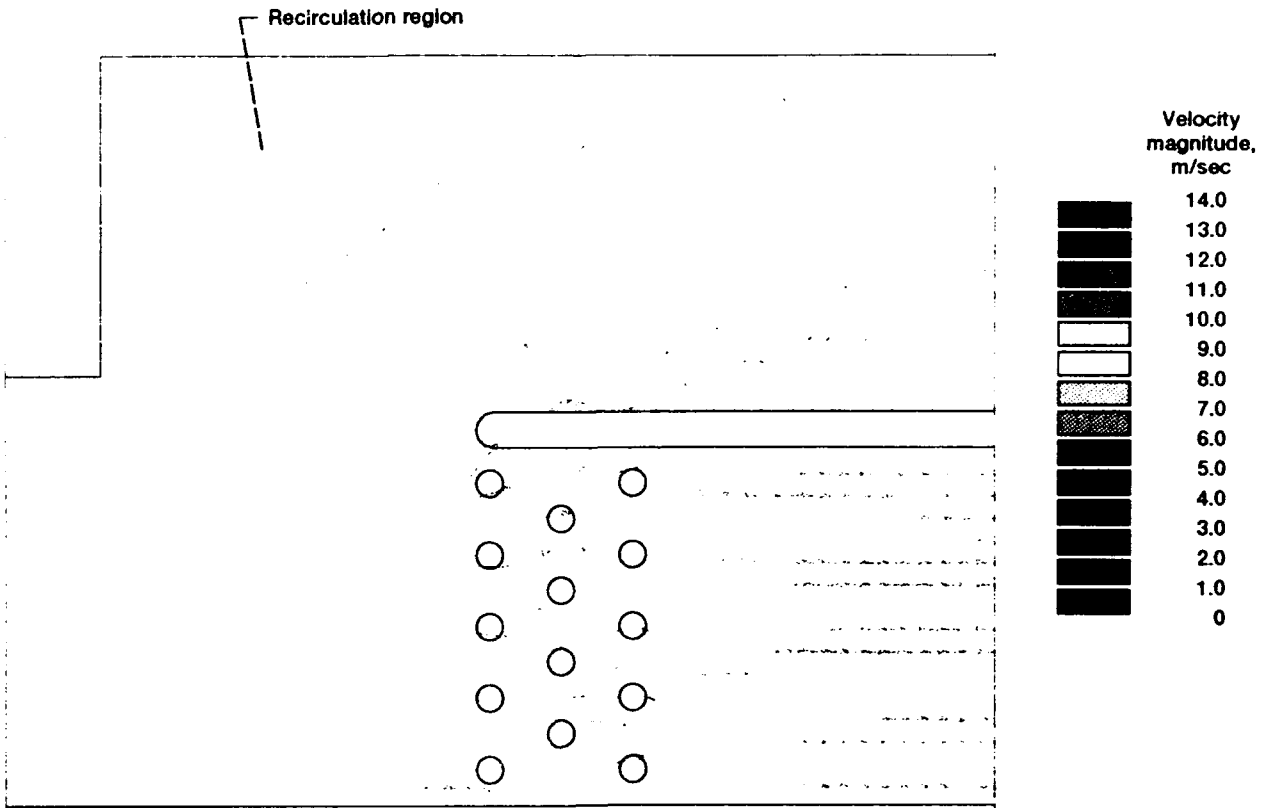


Figure 17.—Computational flow field map; Reynolds number, 45,000.

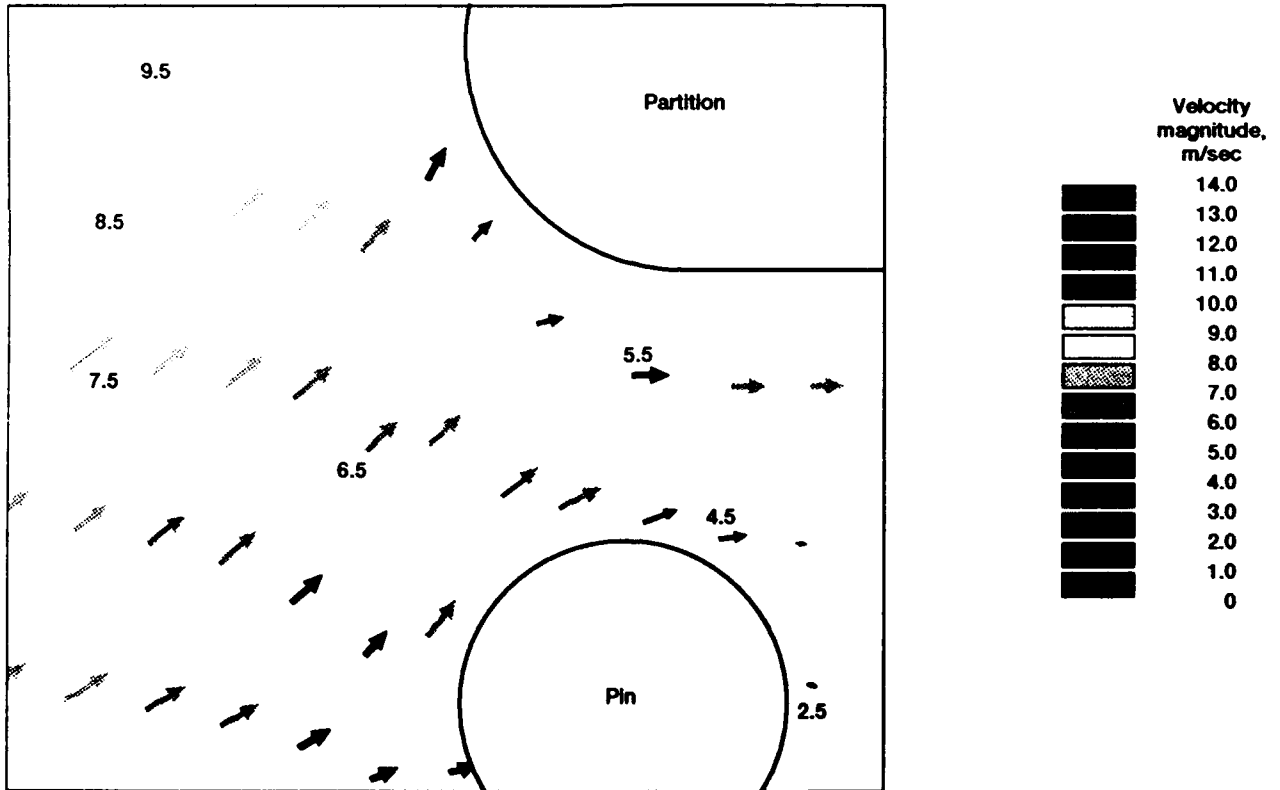


Figure 18.—Computational flow field map; Reynolds number, 45,000. Close-up. (Velocities given in m/sec.)

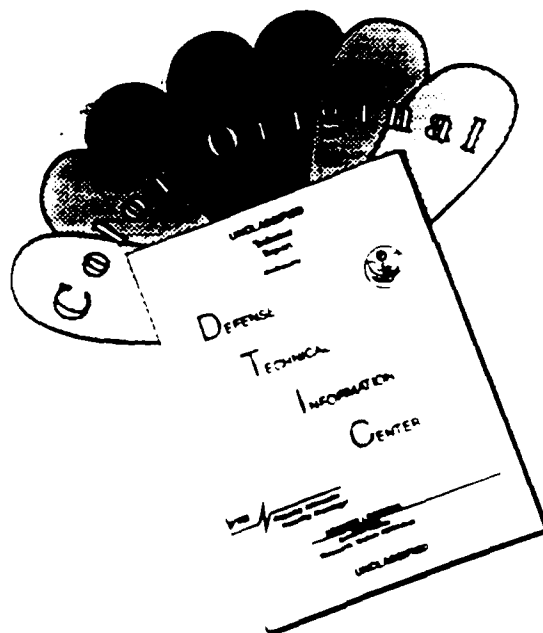
# REPORT DOCUMENTATION PAGE

Form Approved  
OMB No. 0704-0188

Public reporting burden for this collection of information is estimated to average 1 hour per response, including the time for reviewing instructions, searching existing data sources, gathering and maintaining the data needed, and completing and reviewing the collection of information. Send comments regarding this burden estimate or any other aspect of this collection of information, including suggestions for reducing this burden, to Washington Headquarters Services, Directorate for Information Operations and Reports, 1215 Jefferson Davis Highway, Suite 1204, Arlington, VA 22202-4302, and to the Office of Management and Budget, Paperwork Reduction Project (0704-0188), Washington, DC 20503.

<b>1. AGENCY USE ONLY (Leave blank)</b>		<b>2. REPORT DATE</b> June 1993	<b>3. REPORT TYPE AND DATES COVERED</b> Technical Memorandum	
<b>4. TITLE AND SUBTITLE</b> Measurements and Computational Analysis of Heat Transfer and Flow in a Simulated Turbine Blade Internal Cooling Passage			<b>5. FUNDING NUMBERS</b>  WU-505-62-52	
<b>6. AUTHOR(S)</b> Louis M. Russell, Douglas R. Thurman, Patricia S. Simonyi, Steven A. Hippensteele, and Philip E. Poinssatte				
<b>7. PERFORMING ORGANIZATION NAME(S) AND ADDRESS(ES)</b> National Aeronautics and Space Administration Lewis Research Center Cleveland, Ohio 44135-3191			<b>8. PERFORMING ORGANIZATION REPORT NUMBER</b>  E-7894	
<b>9. SPONSORING/MONITORING AGENCY NAME(S) AND ADDRESS(ES)</b> National Aeronautics and Space Administration Washington, D.C. 20546-0001			<b>10. SPONSORING/MONITORING AGENCY REPORT NUMBER</b>  NASA TM-106189 AIAA-93-1797 ARL-MR-91	
<b>11. SUPPLEMENTARY NOTES</b> Prepared for the 29th Joint Propulsion Conference and Exhibit cosponsored by the AIAA, SAE, ASME, and ASEE, Monterey, California, June 28-30, 1993. Louis M. Russell, NASA Lewis Research Center; Douglas R. Thurman, Vehicle Propulsion Directorate, U.S. Army Research Laboratory, Lewis Research Center, Cleveland, Ohio 44135; Patricia S. Simonyi, Sverdrup Technology, Inc., Lewis Research Center Group, 2001 Aerospace Parkway, Brook Park, Ohio 44142; and Steven A. Hippensteele and Philip E. Poinssatte, NASA Lewis Research Center. Responsible person, Louis M. Russell, (216) 433-5896.				
<b>12a. DISTRIBUTION/AVAILABILITY STATEMENT</b>  Unclassified - Unlimited Subject Category 34			<b>12b. DISTRIBUTION CODE</b>	
<b>13. ABSTRACT (Maximum 200 words)</b>  Visual and quantitative information were obtained on heat transfer and flow in a branched-duct test section that had several significant features of an internal cooling passage of a turbine blade. The objective of this study was to generate a set of experimental data that could be used to validate computer codes for internal cooling systems. Surface heat transfer coefficients and entrance flow conditions were measured at entrance Reynolds numbers of 45,000, 335,000, and 726,000. The heat transfer data were obtained using an Inconel heater sheet attached to the surface and coated with liquid crystals. Visual and quantitative flow field results using particle image velocimetry were also obtained for a plane at midchannel height for a Reynolds number of 45,000. The flow was seeded with polystyrene particles and illuminated by a laser light sheet. Computational results were determined for the same configurations and at matching Reynolds numbers; these surface heat transfer coefficients and flow velocities were computed with a commercially available code. The experimental and computational results were compared. Although some general trends did agree, there were inconsistencies in the temperature patterns as well as in the numerical results. These inconsistencies strongly suggest the need for further computational studies on complicated geometries such as the one studied.				
<b>14. SUBJECT TERMS</b> Heat transfer; Flow visualization; Liquid crystals; Turbines; Internal cooling; Particle image velocimetry			<b>15. NUMBER OF PAGES</b> 29	
			<b>16. PRICE CODE</b> A03	
<b>17. SECURITY CLASSIFICATION OF REPORT</b> Unclassified	<b>18. SECURITY CLASSIFICATION OF THIS PAGE</b> Unclassified	<b>19. SECURITY CLASSIFICATION OF ABSTRACT</b> Unclassified	<b>20. LIMITATION OF ABSTRACT</b>	

# DISCLAIMER NOTICE



THIS DOCUMENT IS BEST QUALITY AVAILABLE. THE COPY FURNISHED TO DTIC CONTAINED A SIGNIFICANT NUMBER OF COLOR PAGES WHICH DO NOT REPRODUCE LEGIBLY ON BLACK AND WHITE MICROFICHE.